53rd AIAA Aerospace Sciences Meeting/33rd ASME Wind Energy Symposium, January 5 - 9 2015, Kissimmee, FL

Actuator Line Wind Turbine simulations in Atmospheric Turbulent Flows using Spectral Element Method

Tanmoy Chatterjee*, Yulia Peet†

Actuator line aerodynamics (AL) model is becoming increasingly popular for characterization of the flow field and the turbulent wake created by the rotating turbines. AL model does not require boundary layer resolution of the flow around turbine blades and is thus significantly more efficient than the fully-resolved computations. The current paper aims at performing spectral element simulations of AL model wind turbine response to a realistic neutral atmospheric boundary layer (ABL) flow field. In the present paper, we incorporate the benchmark results of neutral ABL simulations using a rough wall LES model at very high Reynolds number and results of wind turbine response to ABL flows using AL model.

I. Introduction

Interception of incoming flow field by the rotating turbine creates counter-rotating wakes behind the turbine. These wakes are extremely important as their characteristics affect turbines in the second row and beyond. Hence the study of these wakes are essential in order to predict and optimize the performance of wind turbines arranged in a larger wind farm. Moreover, turbulence in the flow field has a strong impact on the wake structure and the effect is generally different depending on whether the turbulent motions are buoyancy-driven or shear-driven. The atmospheric boundary layer (ABL) flows approaching and surrounding the wind turbine are of extremely high Reynolds number ($Re \sim 10^8 - 10^{12}$). Consequently the stringent mesh requirements of direct numerical simulation (DNS) ($N_x \times N_y \times N_z \sim Re^{9/4}$) has rendered the method computationally infeasible for ABL flows.[1–3] Large eddy simulation (LES) of wind turbine arrays is a promising technique with the potential of yielding a reliable data concerning the flow patterns as well as the energy output of turbines in a wind plant. Additionally an LES is justified for such calculations since the LES resolves the spatio-temporal evolution of large scale flow structures faithfully, which are the dominant contributors to the energy generated by wind turbine. Several attempts at characterizing the performance of wind turbine arrays with LES have been undertaken.[4–8]

Reduced-order aerodynamic models representing the effect of the rotating blades on the flow emerged and later evolved due to the computational bottleneck of fully-resolved calculations. The early theories describing the behavior of propellers are known as momentum theory and go back to late 19th century with the works of Rankine,[9] Froude, Drzewiecki and others. It was later extended by Glauert[10] into a blade-element momentum theory (BEM) to account for non-uniformities along the blade, such as shape, chord, twist etc. BEM method was adopted to use with wind turbine simulations as an actuator disk method,[11] and further extended to a generalized actuator disk method.[12,13] Generalized actuator disk method was used in some of the earlier-cited LES studies of wind turbine arrays.[4,5]

Further improvement to a generalized actuator disk method was introduced by Sørensen & Shen[14] and developed by Troldborg[15] in the form of an actuator line aerodynamics (AL) method. The major change with respect to an actuator disk model is abandoning the circumferential symmetry of the induced force field and arriving at a fully three-dimensional model which accounts for the rotating blades as separate rotating lines to correctly predict the rotating wake structure. AL method is currently one of the most advanced model

*School for Engineering of Matter, Transport and Energy (SEMTE), Arizona State University; E-mail: tchatte3@asu.edu

†Assistant Professor, School for Engineering of Matter, Transport and Energy (SEMTE), Arizona State University; E-mail: ypeet@asu.edu

for the rotating blade aerodynamics, as an optimised alternative to computationally intensive fully resolved calculations and has been used in the recent large eddy simulations of Lillgrund wind plant containing 48 turbines by Churchfield et al.[7,8]

Since the current calculation involves extremely high Reynolds number, a decoupled simulation of atmospheric boundary layer has been performed that should be incorporated into the actuator line model. In the present simulations, the atmospheric boundary layer data has been essentially used as an initial condition with periodic streamwise boundary conditions for AL model using standard Smagorinsky eddy viscosity closure in LES with near wall modeling[20–23] modified for rough wall. The use of a periodic streamwise boundary conditions is justified because we are conducting a straightforward study to understand the effect of counter-rotating wake generation subjected to neutral atmospheric turbulent boundary layer. However for a more realistic numerical simulations of AL model turbine response, turbulent inflow boundary conditions should be used from the ABL data. Various advanced inflow-generation techniques in turbulent boundary layer have been discussed in the literature in the past decade, by Spalart,[16] Lund et al.[17] and Ferrante and Elghobashi.[18] These methods were mostly used and validated for smooth wall turbulence with growing boundary layer. For rough wall turbulence, decoupled ABL simulations have also been implemented with periodic streamwise boundary conditions with a buffer zone for stabilizing inflow in actuator line model.[6,19,20] We plan to implement the turbulent inflow boundary condition for our AL model in near future. In our simulations, we use spectral element code Nek5000[24] featuring superior computational efficiency and parallel performance.

II. Numerical Method

Spectral element code Nek5000[24] is used to solve the 3D Navier-Stokes (NS) equation for both the actuator line model turbine response and atmospheric boundary layer simulation. Spectral element method (SEM) is a high-order weighted residual technique that combines the geometric flexibility of finite elements with the rapid convergence and tensor-product efficiencies of global spectral methods.
In the spectral element formulation the computational domain $\mathbf{\Omega} = \cup_{k=1}^{K} \mathbf{\Omega_k}$. Each $\mathbf{\Omega_k}$ is the image of reference subdomain under a mapping $\mathbf{x}^k(\mathbf{r}) \in \mathbf{\Omega_k} \rightarrow \mathbf{r} \in \hat{\mathbf{\Omega}}$, with a well defined inverse $\mathbf{r}^k(\mathbf{x}) \in \hat{\mathbf{\Omega}} \rightarrow \mathbf{x} \in \mathbf{\Omega_k}$, where the reference subdomain $\hat{\mathbf{\Omega}} = [-1,1]^d$ with d being the dimension of the problem. Scalar functions with each element $\mathbf{\Omega_k}$ are represented as N^{th} order tensor product polynomials on a reference subdomain $\hat{\mathbf{\Omega}}$. In 3D, any function in the spectral element method in the local element can be expressed as follows

$$f(x)|_{\mathbf{\Omega_k}} = \sum_{m=1}^{N_x} \sum_{n=1}^{N_y} \sum_{p=1}^{N_z} f_{mnp}^k h_m(r_1) h_n(r_2) h_p(r_3), \quad r_1, r_2, r_3 \in [-1,1]^3 \tag{1}$$

where, $h_i(\mathbf{r})$ is the Lagrange polynomial of degree N_x,N_y or N_z satisfying $h_i(\zeta_j) = \delta_{ij}$, where $\zeta = [-1,1]$ and δ_{ij} is the Kronecker delta function. Usually, the polynomial chosen is orthogonal in nature (a solution of Sturm Liouville problem) to obtain least square interpolation error from generalized Fourier series construction. In Nek5000, the orthogonal polynomial used is Legendre polynomial and $\zeta_j, j = 1, N_x$ (for x direction and similarly likewise) are the Gauss-Lobato-Legendre (GLL) points of quadrature.
The time discretization of NS solver in Nek5000 involves k^{th} order backward difference/extrapolation scheme (BDF/EXT) where $k = 2$ or 3. The code is fully dealiased using 3/2 rule,[25,26] the velocity is solved using preconditioned conjugate gradient (CG) method and the pressure solver uses iterative generalized mean residual solver (GMRES) method in Krylov subspace. The current algorithm was optimized to achieve perfect scalability in parallel implementation up to 1,000,000 processors.[27,28]

II.A. Large Eddy Simulation

The filtered Navier-Stokes equations registering the spatio-temporal evolution of large-scale structures of the flow have been solved in the computational domain both for the neutral atmospheric boundary layer simulations as well as actuator line model in spectral element methods.

$$\frac{\partial \tilde{u}_i}{\partial t} + \tilde{u}_j \frac{\partial \tilde{u}_i}{\partial x_j} = -\frac{1}{\rho}\frac{\partial \tilde{p}}{\partial x_i} + \nu \frac{\partial^2 \tilde{u}_i}{\partial x_j \partial x_j} + \frac{1}{\rho}\frac{\partial \tau_{ij}^{SGS}}{\partial x_j} + \frac{\widetilde{f}_i}{\rho} \tag{2}$$

$$\frac{\partial \tilde{u}_i}{\partial x_i} = 0 \tag{3}$$

As seen in Equation(2), the Subgrid-scale (SGS) stress arises from the non-commutativity of the filtering applied to the non-linear advection term and needs proper closure to solve Navier-Stokes equation. The"tilde" denotes the filtering applied on the velocity and pressure variables (u_i, p). Smagorinsky type eddy-viscosity models have been used for SGS stress closure analogous to viscous stresses.

$$\frac{1}{\rho}(\tau_{ij}^{SGS} - \frac{1}{3}\tau_{kk}^{SGS}\delta_{ij}) = -2\nu_t \widetilde{S}_{ij} \tag{4}$$

The eddy viscosity ν_t can be formulated as $\nu_t = (C_s\Delta)^2|\widetilde{S}|$, with $|\widetilde{S}| = \sqrt{2\widetilde{S}_{ij}\widetilde{S}_{ij}}$ (See Section II.B for details of choice of C_s, Δ). The forcing term $\widetilde{f}_i$ in ABL represents the mean pressure gradient that drives the flow. The LES of atmospheric boundary layer simulations have been carried out at $Re = 10^{10}$, where Reynolds number is based on the boundary layer thickness (see Section III.A). For, simulations with the acutator line model, a different set of non-dimensionalization is prescribed which requires the Reynolds number to be based on the turbine-rotor radius length, and amount to $Re \sim 10^9$. The forcing term $\widetilde{f}_i$ in actuator line model represents the thrust, lift and drag forces experienced by the fluid through the actuator lines. Since the computational domain here is of a short span (not a wind farm as in [5, 7]), we have chosen to ignore the coriolis forces.[23,29] The simulation being performed for neutral atmospheric boundary layer also ensures that the heat flux $q = 0$ at the bottom wall, and the buoyancy forces are neglected.[19,30]

II.B. Neutral Atmospheric Boundary Layer Simulations

The current simulation deals with generating a feasible ABL flow field that is intercepted by the wind turbine. The simplest case is the neutral ABL simulations, where the turbulence is generated from the shear in the flow over rough wall terrain. Our present model uses x as the streamwise direction, y as the spanwise direction and z as the wall normal direction in a cartesian framework as discussed in section III. The mean streamwise velocity profile of ABL in the surface layer (roughly $10 \sim 20\%$ of boundary layer)[23,29,31] can be given as

$$\bar{U}(z) = \frac{u_\tau}{\kappa}\ln\frac{z}{z_0} + \frac{u_\tau}{\kappa}\psi_m(\frac{z}{L_M}), \quad z \gg z_0 \tag{5}$$

where, u_τ is the friction velocity scale, z_0 is the aerodynamic roughness length and $\kappa = 0.4$ is the Von Karman constant, ψ_m is a non dimensional momentum stability function and L_M is stability length scale by Monin and Obukhov.[31,32] For neutral ABL, $L_M \to \infty$ and hence the mean velocity profile is essentially logarithmic in nature in the surface layer[32] with $\psi_m \to 0$.

The boundary layer (BL) thickness for flat plate type of turbulent flows can be usually expressed as $\delta/x \sim Re_x^{-p}$, where p is very close to 1 ($p = 0.8$ for turbulent flow over smooth flat plate).[33] Consequently, the streamwise growth of the turbulent BL, could be expressed as $d\delta/dx \sim Re_x^{-(1+p)}$. Since $Re_x \approx 10^8 - 10^{12}$ for ABL flows, the growth of the turbulent BL $d\delta/dx \approx 0$ rendering periodic boundary condition in the homogeneous streamwise direction feasible. The spanwise boundary conditions are periodic since it is consistent with the physics of the flow. The top boundary condition is a stress free lid similar to the flat plate flow, i.e., $d\tilde{u}_x/dz = d\tilde{u}_y/dz = \tilde{u}_z = 0$. For extremely high Re ABL flows, the viscous sublayer $\delta_\nu/\delta \sim O(Re_\tau^{-1}) \approx 0$, and the aerodynamic roughness $z_0 \gg \delta_\nu$. Since the viscous layer cannot be resolved in such simulations, the use of shear-stress boundary conditions as near-wall modelling LES becomes imperative. Consequently, the bottom rough wall model for ABL has been developed from the log-law of the wall coupled with Monin-Obukhov similarity theory[32] and near wall shear stress model of Schumann[22] and was further used by Businger et al.,[31] Moeng [30] and Stoll and Porté-Agel .[19] The rough wall model in collocated SEM (Equation(6)) calculates instantaneous (filtered) surface shear stress as a function of explicitly filtered velocity at the lowest grid point.[5,29,34] The "tilde" represents implicit grid filtering in LES, while in SEM, the explicit filtering represented by the "hat" is carried out in modal space by attenuating two-highest Legendre polynomial modes. The explicit filtering is done in an effort to minimize the log-layer mismatch (overshoot of slope of logarithmic mean velocity profile observed in high Re flows) .[29,34,35]

$$\tau_{i,zs} = -\kappa^2 \frac{\widehat{\widetilde{u}}_r(x, y, z = \frac{\Delta z}{2}, t)\widehat{\widetilde{u}}_i(x, y, z = \frac{\Delta z}{2}, t)}{[\ln(z = \frac{\Delta z}{2}/z_0)]^2} \tag{6}$$

where, $i = x, y$ with $\widehat{\widetilde{u}}_r(x, y, z = \frac{\Delta z}{2}, t) = \sqrt{\sum_{i=x,y} \widehat{\widetilde{u}}_i(x, y, z = \frac{\Delta z}{2}, t)^2}$ with $\widehat{\widetilde{u}}_{i,r}(x, y, z = \frac{\Delta z}{2}, t) = \frac{1}{2}(\widehat{\widetilde{u}}_{i,r}(x, y, 0, t) + \widehat{\widetilde{u}}_{i,r}(x, y, \Delta z, t))$ and $\ln(z/z_0)|_{z=\frac{\Delta z}{2}}$ as seen are computed at the mid-point (interpolated value) between $z = 0$ and Δz, with Δz being the height of the first node away from the wall. Earlier cited literature on rough-wall models[19,29–31] have generally used staggered finite-difference schemes when using stress boundary conditions for rough wall models. Since the present paper incorporates the first study of rough wall models that we are aware of, using collocated spectral elements, certain modifications in the conventional rough-wall models of the cited-researchers have been introduced in Equation(6). z_0 is the aerodynamic roughness length of the bottom wall surface, $\kappa = 0.4$ (Von Karman Constant) and subscript s is the surface value.

The aerodynamic roughness length z_0 is a monotonic measure of physical surface roughness h and their empirical relations are discussed in literature.[36–39] The friction velocity scale is given by $u_\tau = \sqrt{\tau_w/\rho}$, where τ_w is the wall shear stress, $-dp/dx$ is the streamwise pressure gradient that drives the ABL flow, L_z is the wall-normal computational domain size and ρ is the fluid density, which can be further simplified as follows.

$$\rho {u_\tau}^2 = \tau_w = \sqrt{\tau_{x,zs}^2 + \tau_{y,zs}^2} = \kappa \frac{\widehat{\widetilde{u}}_r(x, y, z = \frac{\Delta z}{2}, t)}{\ln(z = \frac{\Delta z}{2}/z_0)} \sim (-\frac{dp}{dx})L_z \tag{7}$$

A proper choice of the subgrid-scale model with wall damping used in LES simulations with near wall modelling is essential, since the proper dissipation characteristics of the SGS model, generate accurate subgrid scale stresses, and kinetic energy which is necessary for generating the log-law profile and correct second order statistics near the wall.[23,29,40]

In the current study we use Smagorinsky type eddy-viscosity model with algebraic wall damping (Equation(8)) to take into account stochastic backscatter which has been used from Mason and Thompson (1992)[35] especially designed for suppressing log-layer mismatch of rough-wall high Re flows.

$$\frac{1}{(C_s\Delta)^n} = \frac{1}{(C_0\Delta)^n} + \frac{1}{\kappa(z + z_0)^n} \tag{8}$$

The Smagorinsky eddy viscosity model is simple in terms of its implementation, although we plan to incorporate more sophisticated models like Lagrangian scale-dependant dynamic Smagorinsky model,[23]scale adaptive Smagorinsky model[29] in near future. From the literature,[23,29] usually $n = 2$, and $C_0 \approx 0.10$ has been used for a smooth blending function retrieving mixing length scales $\sim \kappa z$ corresponding to the log-law of the wall. In Equation(8), C_s is the Smagorinsky coefficient and Δ is the grid-filter width. In the current spectral element method, we use $\Delta = (\Delta_x\Delta_y\Delta_z)^{1/3}$ with $\Delta_x, \Delta_y, \Delta_z$ being calculated as central difference between the GLL nodes and one-sided difference at the boundaries followed by an average across inter-element boundaries.[41] Since spectral element methods are much less dissipative and dispersive, an optimal value of $C_0 \approx 0.15$ has been chosen to stabilize the statistics without incurring too much diffusion.

II.C. Actuator Line Model: Turbine Response

Actuator line model was first developed by Sørensen & Shen[14] and Troldborg,[15] later used by Churchfield et al.[7,8] in finite volume computations and was developed for the current spectral element code by Peet et al.[42] The idea of the actuator line model is that the influence of the rotating blades is modelled as a sum of discrete body forces introduced into the flow field. Thus, resolving boundary layer around the blades can be avoided, and simple rectilinear grid can be used. In an actuator line model, the blades are divided into the elements, similar to BEM, and the local lift (L) and drag (D) force experienced by each element is calculated as

$$L = \frac{1}{2} C_l(\alpha)\, \rho\, V_{rel}^2\, c\, w, \tag{9}$$

$$D = \frac{1}{2} C_d(\alpha)\, \rho\, V_{rel}^2\, c\, w, \tag{10}$$

where $C_l(\alpha)$ and $C_d(\alpha)$ are the lift and drag coefficients respectively, α is the local angle of attack, ρ is the fluid density, V_{rel} is the local velocity magnitude relative to the rotating blade, c is the local chord length, and w is the actuator element width. Considering velocity triangles for the rotating blade,[14,15] as shown in Figure 1 the local relative velocity magnitude V_{rel} can be given as

$$V_{rel} = \sqrt{V_x^2 + (\Omega\, r - V_\theta)^2}, \tag{11}$$

where, Ω is the rotor rotational speed, V_x and V_θ are the velocity components in the axial direction x (perpendicular to the plane of rotation), and in circumferential direction (in the plane of rotation corresponding to yz plane) respectively, r is the radial coordinate of the actuator element. Local angle of attack α is computed as $\alpha = \phi - \gamma$, where ϕ is the angle between the relative velocity V_{rel} and the rotor plane

$$\phi = \tan^{-1}\left(\frac{V_x}{\Omega\, r - V_\theta}\right) \tag{12}$$

and γ is the local pitch angle. The element lift and drag coefficients $C_l(\alpha)$, $C_d(\alpha)$ as function of α can be determined from the lookup tables. After calculating the local aerodynamic force $\vec{f} = L\vec{e_L} + D\vec{e_D}$, its

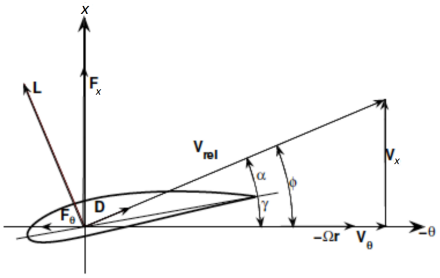

Figure 1: Velocity triangle for the determination of the local relative velocity on a turbine blade.

influence, $-\vec{f}$, on the flow is incorporated as a sum of discrete forces (here $\vec{e_L}$ and $\vec{e_D}$ are the unit vectors in the direction of the local lift and drag, respectively). The total force from all the blade elements experienced by the fluid is given by

$$\vec{F}(x,\, y,\, z,\, t) = -\sum_{i=1}^{N} \vec{f}(x_i,\, y_i,\, z_i,\, t)\, \delta(|\vec{r} - \vec{r_i}|) \tag{13}$$

where, $\delta(|\vec{r}-\vec{r_i}|)$ is the Dirac delta function. Equation(13) represents the discrete force model in a continuous form by using delta function. To avoid singularities, the forces are distributed smoothly on several mesh points by using the Gaussian weight function (smeared out delta function),

$$\eta_\epsilon(d) = \frac{1}{\epsilon^3 \pi^{3/2}} \exp\left[-\left(\frac{d}{\epsilon}\right)^2\right], \tag{14}$$

with the modified force term as

$$\vec{F}(x,\, y,\, z,\, t) = -\sum_{i=1}^{N} \vec{f}(x_i,\, y_i,\, z_i,\, t)\, \eta_\epsilon(|\vec{r} - \vec{r_i}|), \tag{15}$$

where the summation is over all N blade elements, x_i, y_i, z_i are the local coordinates of each blade element, and $|\vec{r}-\vec{r_i}|$ is the distance between the current point in the flow and the center of the blade element. Several studies have been carried out for the choice of an optimal Gaussian width ϵ.[15,43] The value of $\epsilon = 2\,w$ proposed by Troldborg[15] is used in the current study.

III. Computational Setup

III.A. Neutral Atmospheric Boundary layer simulations

The computational domain of the neutral ABL simulation is of rectangular geometry and cartesian spectral element collocated mesh has been used for such calculations. We model a similar setup as in Ref. 20, 44 in an effort to make comparison with their results. In the present cartesian framework, x is the streamwise direction, y is the spanwise direction and z is wall normal direction as shown in Figure 2. The computational domain for the ABL simulations is $4\pi\delta \times 2\pi\delta \times 2\delta$, where $L_x = 4\pi\delta$, $L_y = 2\pi\delta$, and $L_z = H = 2\delta$ is the boundary-layer thickness. The domain is uniformly discretized into $30 \times 20 \times 24$ elements in $x, y,$ and z directions respectively. With 8^3 GLL points per element, the number of grid points for the ABL simulations is $211 \times 141 \times 169 \approx 5 \times 10^6$. The rough-wall closure and subgrid scale (SGS) eddy-viscosity models used for the large eddy simulations of ABL model are described in Section II.B.

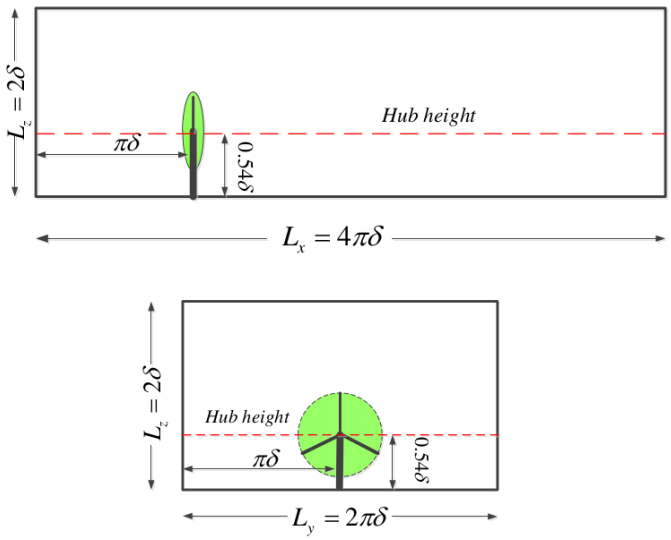

Figure 2: Computational domain for neutral ABL and wind turbine AL simulations. top: $x-z$ plane, bottom: $y-z$ plane

III.B. Actuator Line Simulations

The boundary conditions and the domain size remain the same as in Section III.A with the statistically stationary ABL simulation serving as an initial condition to the actuator line model. The domain size is rescaled in terms of turbine rotor radius (diameter) is given as $31.5R \times 16R \times 5R$ ($15.75d \times 8d \times 2.5d$), where $R = 0.4\delta$ is the radius of the turbine-rotor ($d = 2R$ is turbine-rotor diameter). As in Ref. 20, 44, the rotor-centre of the turbine is placed at $\pi\delta \times \pi\delta \times 0.54\delta$ or $8R \times 8R \times 1.35R$ ($4d \times 4d \times 0.675d$). The simulations are run with tip-speed ratio $\lambda = 5.05$, (the typical tip-speed ratio for wind turbine is $3-8$) where $\lambda = \Omega R/\overline{V}_x$, with Ω being the angular velocity of rotor, and $\overline{V}_x$ is the bulk mean stream wise velocity. The pitch angle used in the current simulation γ varies linearly between $0^\circ - 10^\circ$ along the span and the chord-length varies as $C \sim 0.03R - 0.11R$, with various NACA aerofoils being used for the blade corresponding to the study of Troldborg.[15] The flow velocities at the location where lift and drag forces on the blades are acting are obtained from spectral interpolation technique in Nek5000.[41] The drag forces experienced by the nacelle and turbine tower has been neglected in the current simulations. The subgrid-scale model remains the same as in Section II.B. However, in the AL model,[15,42] it was observed that approximately 30 points were required in the blade-span ($y-z$ direction) to resolve the wake, demanding a local refinement of the grid of ABL domain near the turbine.[4] Simultaneous refinement in the streamwise direction is also of crucial importance, as far as resolving the wake is concerned. It was observed, that without proper resolution in the streamwise direction, spurious modes develop upstream of the turbine, which propagate almost half the distance up-stream eventually polluting the upstream flow. The discretization of the actuator line domain can be written as $50 \times 26 \times 24$ elements with refined elements in spanwise y direction and stream-wise x direction near the turbine with the number of grid-points amounting to $451 \times 235 \times 217 \approx 22 \times 10^6$ (10^3 GLL points per element). Additionally, nodal interpolation filter of spectral accuracy[45] has been applied on the two highest modes to completely eliminate the spurious modes. The aerodynamic roughness is taken to be $z_0 = 10^{-4}\delta$ (constant similar to [20,23]) for both neutral ABL simulations (Section III.A) and actuator line simulations (Section III.B). The first grid node away from the wall is $\Delta z > z_0$ by a factor of $20-30$ for both the simulations and is expected to fall into the logarithmic wall layer for such high Reynolds number. In the current approach, the boundary conditions for both ABL simulations and AL simulations remain the same, and the statistically stationary flow of the ABL model has been supplied into the actuator line simulations as an initial condition.

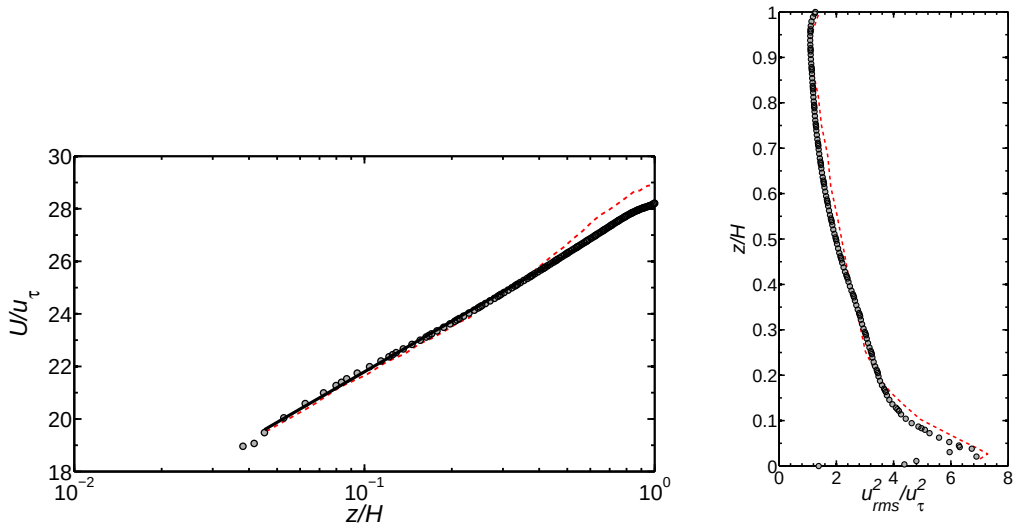

(a) (b)

Figure 3: (a) mean velocity profile in ABL simulations at $Re = 10^{10}$. grey $\circ$, current simulation (SEM); $--$ red, Porté-Agel et al.,[23] 4^{th} order finite-difference, Fourier spectral; $-$ black, a least-squares fit. Expected logarithmic trend in lower $10-20\%$ of the boundary layer ($z/H \sim 0.1$). Resolved Second-order statistics (b) u_{rms}: grey $\circ$, present simulation(SEM); $--$ red, Porté-Agel et al.,[23] 4^{th} order finite-difference, Fourier spectral.

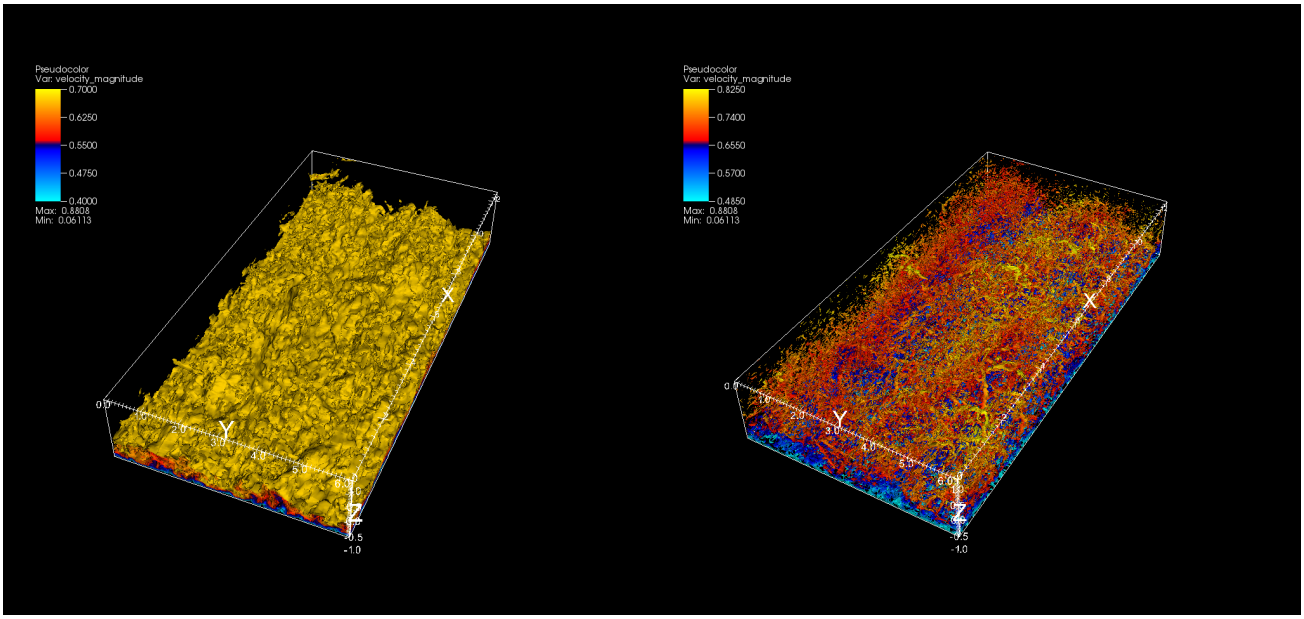

(a) (b)

Figure 4: Neutral ABL simulations at $Re = 10^{10}$ (a) Iso-srufaces of velocity coloured by velocity magnitude showing large-scale bulges (near-wall turbulence close to hub-height 0.54δ) (b) Iso-surfaces of vorticity coloured by velocity-magnitude depicting anisotropic eddies, hairpins.

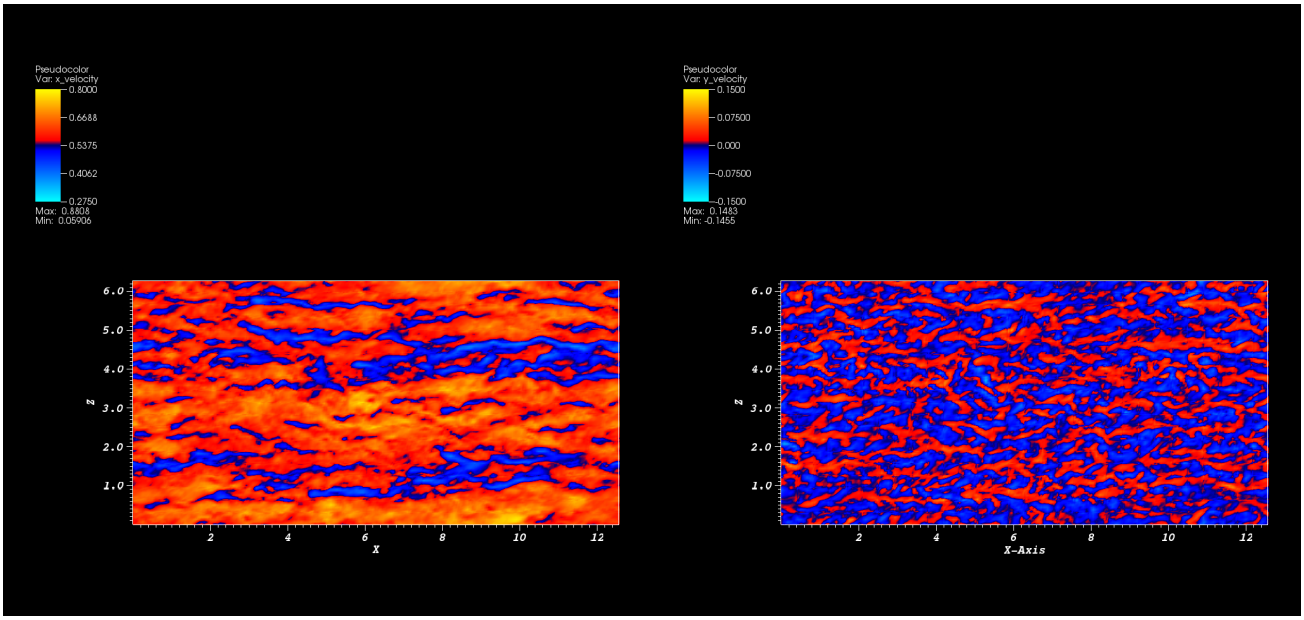

(a) (b)

Figure 5: Neutral ABL simulations at $Re = 10^{10}$ (a) streamwise velocity contours showing low-speed streaks at logarithmic layer (b) wall normal velocity contours showing less anisotropy in the logarithmic layer.

IV. Results

The results describing the actuator line aerodynamic model of wake structure past wind turbines under the influence of turbulent atmospheric boundary layer are presented in the current section. The ABL simulation has been run up to a time sufficiently long, such that it attains statistically stationary turbulent characteristics. Figure 3a shows the statistically stationary streamwise velocity profile normalised by u_τ of neutral ABL simulations, and the logarithmic trends in the profile, obtained through the least squares fit. Figure 3b presents the second order turbulent statistics normalised by wall variable u_τ. The wall normal distance has been normalized with boundary layer thickness $H = 2\delta$. All the statistics in Figure 3 have been compared against the neutral ABL simulations of Porté-Agel et al. as in Ref. 23 and have been shown to agree quite well. Additionally, Figure 4, 5 showing the iso-surfaces of velocity (Figure 4a) and vorticity magnitude (Figure 4b) and low-speed velocity streaks (Figure 5a, 5b)[7,30] of turbulent flow field, gives a qualitative overview of the anisotropic large scale flow structures of neutral ABL being captured by the Smagorinsky eddy viscosity model.

Before moving on to the results of actuator line simulations with atmospheric boundary layer flow, we present the validations of the AL model using Tjæreborg turbine in spectral element methods using uniform inflow conditions with the data of Troldborg.[15] Figure 6 shows that the wake, time-averaged axial interference factor $\langle a_x \rangle$ and the power coefficient C_p are a reasonable match with the thesis of Troldborg.[15] It is intriguing to note, that the wake profiles in Figure 10a shows the best match with the Troldborg data when the number of GLL points in each of x, y and z direction per element is 6.

For the actuator-line simulations in neutral ABL, the iso-surface plots of vorticity are taken at two different snapshots of nondimensional time, $tR/U_{hub} \simeq 10$ and 20 (R is the rotor radius and U_{hub} is the mean-streamwise velocity at hub-height) as shown in Figure 7. At the initial snapshot (Figure 7a), the helical ribbed structures of vorticity downstream of the turbine are visible, while at higher time (Figure 7b), the wakes become vigorously turbulent, with large hairpin structures visible oriented in different direction near the wake. Figure 8 shows different snap-shots at three orthogonal planes depicting the development of the wake. The contour plots clearly reveal the low-velocity wake region (in blue) from Figure 8a–8c, and Figure 8g–8i surrounded by the atmospheric turbulence in red-yellow. Figures 8a–8c also indicate the interaction of the wake with the near-wall dynamics. The meandering nature of the wakes[7] is further depicted in the streamwise-spanwise $x - y$ plane as shown in Figure 8g–8i. An estimation of the power generated

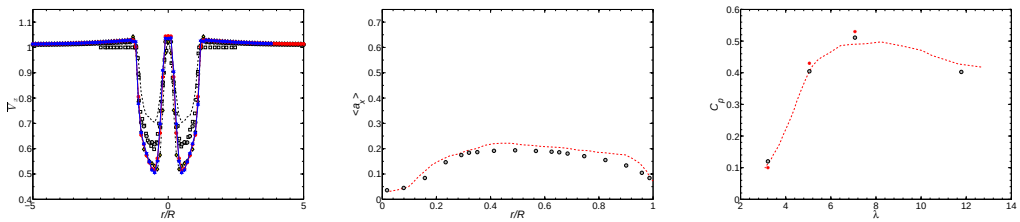

(a) (b) (c)

Figure 6: AL simulations with uniform inflow at $Re = 10^5$ (a) wake velocity profile in the stream-wise direction at station $x/R = 3$ with $\lambda = 5.05$, $--$ black, lx1 = 5; gray $\circ$, lx1=6; yellow $-.\diamond$ lx1=7; red $-\circ$, lx1=8; blue $-\star$,lx1=9 (lx1 is the GLL point per element); white $\square$, Troldborg.[15] (b) time-averaged axial interference factor $\langle a_x \rangle = 1 - \bar{V}_x/V_\infty$ at the rotor plane. grey $\circ$, current computation at lx1=7. red $--$ Troldborg.[15] (c) Power-coefficient (C_p) vs tip-speed ratio (λ) at lx1=7. red $-$, experiment from the thesis of Troldborg;[15] grey $\circ$, Troldborg[15] numerical computations; red $*$, current computation (SEM))

from the turbine and the axial blade-loads can be further obtained from power and thrust coefficients C_p, C_T as depicted in Figure 9. The temporal variation of power coefficient is $C_p \sim 30\%$ (less than inviscid Betz limit of 59%) and thrust coefficient is $C_T \sim 70\%$ in the statistically stationary region (Figure 9a) with low frequency contributions coming from the periodically rotating turbine loads and high frequency fluctuating components coming from turbulence (Figure 9b).

Further plots of the time-averaged streamwise wake velocity profiles at different stream-wise stations $x/d = 2, 3, 5, 7, 10$ can be found in Figure 10 for a qualitative comparison with Wu and Porté-Agel.[20] Qualitative comparisons of stream-wise velocity profile of current simulations can only be done with the data of Wu-and Porté-Agel in the present paper, since we perform the simulations with streamwise boundary conditions for preliminary analysis, while Wu and Porté-Agel[20] have used streamwise periodic boundary conditions with a buffer-region for emulating stabilised inflow conditions. Moreover, our streamwise domain is slightly less than that of Wu and Porté-Agel from a non-dimensional perspective, to fit into our computational resources and our present Reynolds number is almost 4 orders of magnitude larger than the Reynolds number of Wu and Porté-Agel.[20] We plan to present a thorough comparison with the data of Wu and Porté-Agel[20] in the near future. The present wakes are plotted on the top of ABL velocity profile for understanding their intensity and analysing their deviation from the logarithmic trend. Conspicuous wakes could be observed near the hub of the turbine-rotor region depicting high momentum losses with their intensity decaying as we move away from the turbine location in the streamwise direction. Slight discrepancy in the shape of the wake at streamwise station $x/d = 2$ in comparison to the data of Wu and Porté-Agel [20] can be noticed, which can be ascribed to the fact that we did not consider drag in the nacelle region. Small bulges deviating from the logarithmic velocity profile can also be observed beyond the turbine, which can be attributed to constant stream-wise mass flux along with stream-wise periodic boundary conditions.

Time-averaged snapshots of velocity magnitude contours can be observed in Figure 11 showing the mean structures of the wake cores. $x - y$ plane snapshot (Figure 11c) indicates the symmetric nature of the developing wake due to spanwise (y) periodic boundary condition. The $y - z$ plane snapshot (Figure 11b) also indicates low-velocity circular wake region behind the turbine, spanning the entire turbine radius.

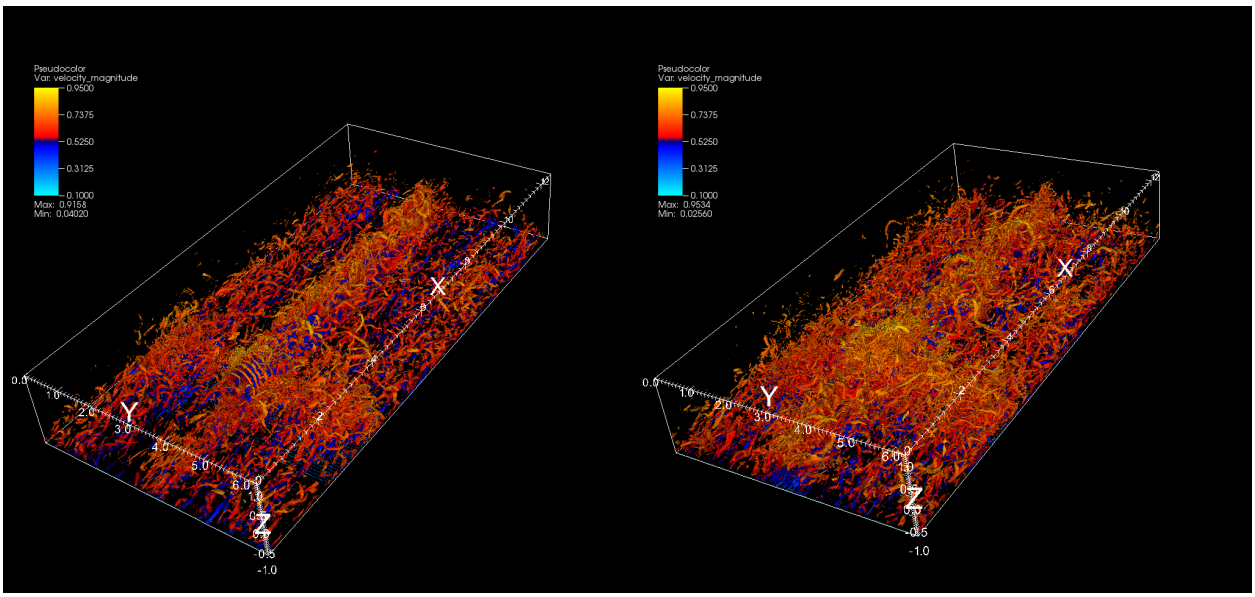

(a) (b)

Figure 7: ABL-AL simulations at $Re = 10^9$ (based on the rotor radius) (a) Iso-surfaces of vorticity at $tR/U_{hub} = 20$ (b) Iso-surfaces of vorticity at $tR/U_{hub} = 40$ (coloured by velocity magnitude)

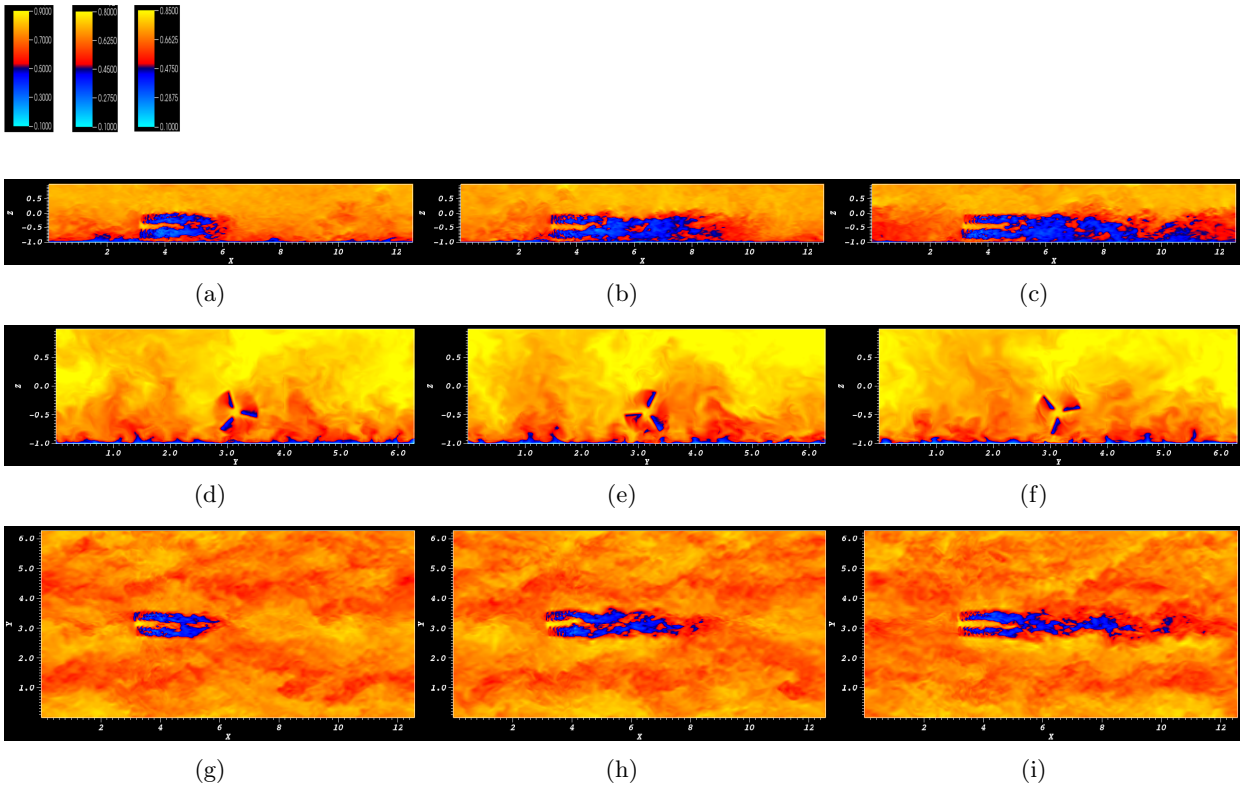

(a) (b) (c)

(d) (e) (f)

(g) (h) (i)

Figure 8: ABL-AL simulations at $Re = 10^9$ (based on the rotor radius). (a)-(c)velocity magnitude in $x - z$ plane; (d)-(f)velocity magnitude in $y - z$ plane; (g)-(h)velocity magnitude in $x - y$ plane. (a), (d), (g) represents snapshots at $tR/U_{hub} = 5$, (b), (e), (h) at $tR/U_{hub} = 12.5$ and (c), (f), (i) at $tR/U_{hub} = 20$. top-left corner: legend of $x - z$, $y - z$ and $x - y$ plane snapshots. Snapshots are obtained by slicing plane at turbine location.

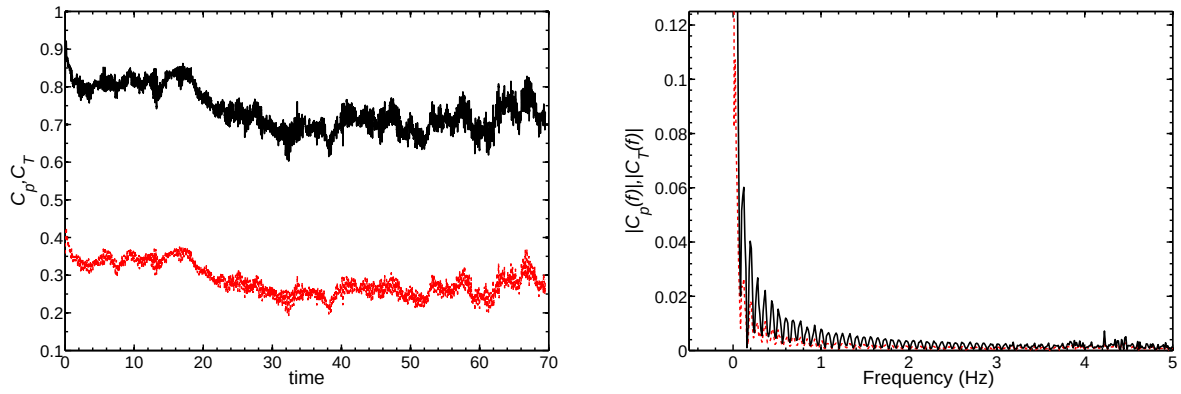

(a) (b)

Figure 9: coefficient of power and thrust (C_p, C_T) for ABL-AL simulations at $Re = 10^9$ (based rotor radius) (a) Temporal variation of power and thrust coefficients (b) Frequency spectrum of power and thrust coefficients. $-$ black, C_T; $--$ red, C_p

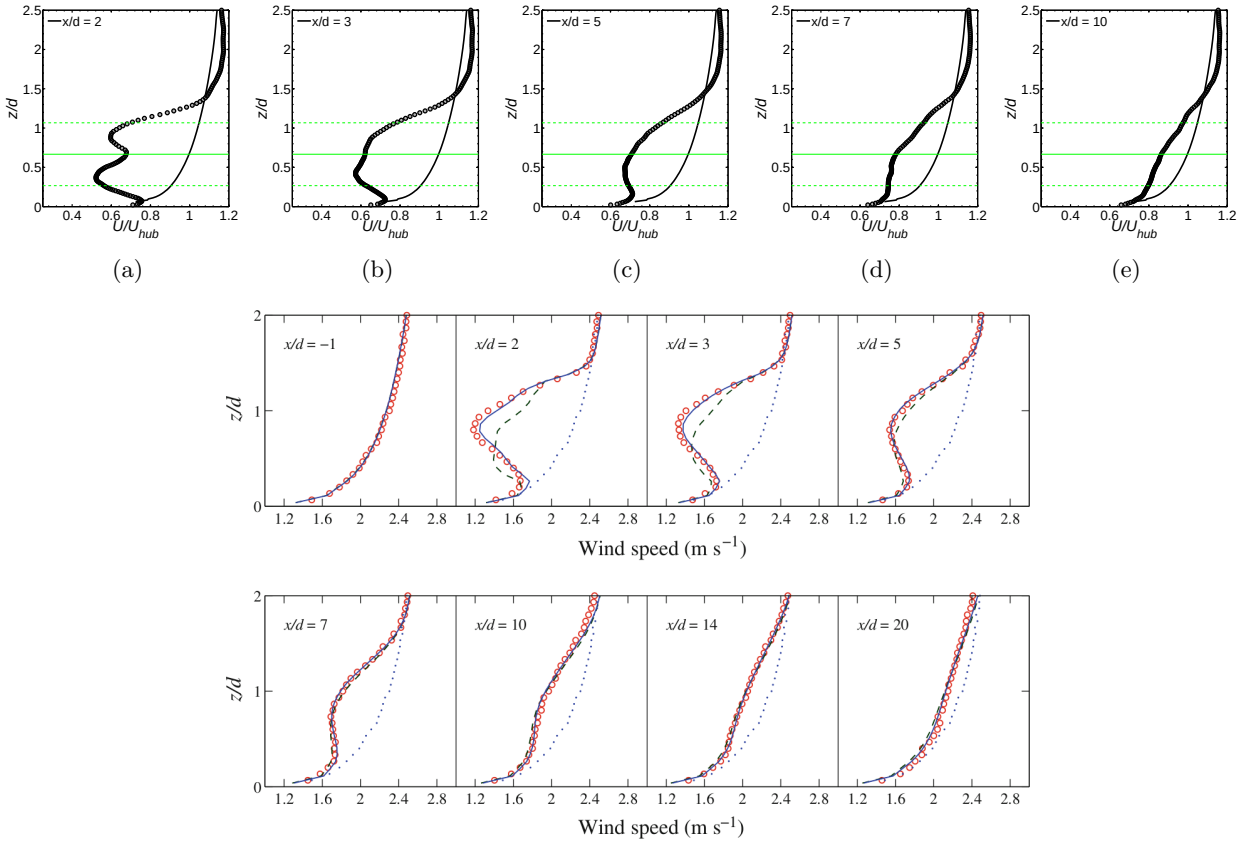

(a) (b) (c) (d) (e)

(f)

Figure 10: ABL-AL simulations at $Re = 10^9$ (based on the rotor radius). (a)-(e) are time averaged axial velocity profile at different stream-wise stations, $x/d = 2, 3, 5, 7, 10$ from the turbine -rotor position (d is the turbine diameter). $-$ green indicates the turbine hub location and $--$ green indicates the span of the turbine-rotor. (f) stream-wise velocity profile at same stations by Wu and Porté-Agel[20] for qualitative comparison (reproduced from their publication).

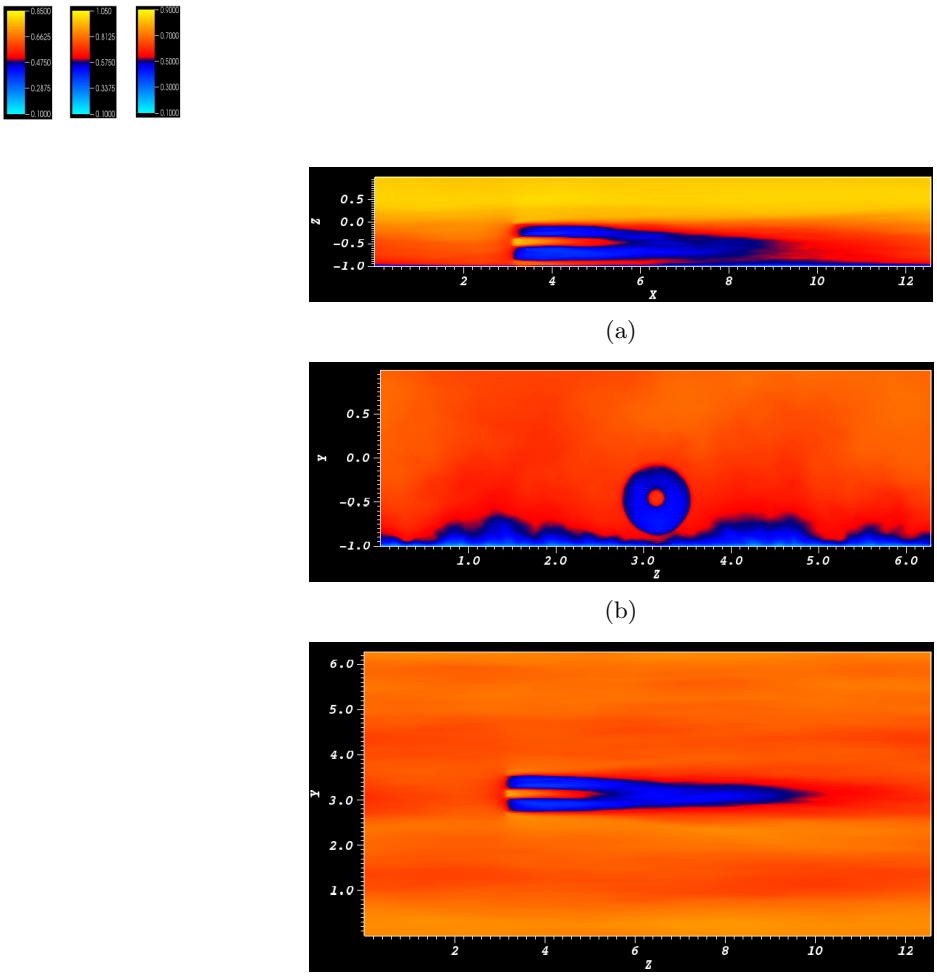

Figure 11: Time-averaged snapshots of velocity profiles of ABL-AL simulations at $Re = 10^9$ (based on the rotor radius).(a) $x-z$ plane (b) $y-z$ plane (c)$x-y$ plane. Top-left corner: legend of $x-z$, $y-z$ and $x-y$ plane time-averaged snapshots. Snapshots are obtained by slicing plane at turbine location.

V. Conclusions and Future Work

In the present paper we have implemented actuator line model coupled with atmospheric boundary layer simulations in exponentially accurate spectral element code Nek5000. The actuator line model has been validated with uniform inflow conditions using Tjæreborg turbine with the thesis of Troldborg[15] which indicates a reasonable match. The atmospheric boundary layer simulations have been further validated by using the data of Porté-Agel et al.[23] indicating the robustness of our ABL model. The simulations involving ABL-AL model with streamwise periodic boundary conditions can be seen as a prefatory analysis of wind turbine AL model response subjected to turbulent atmospheric bundary layer flow, and a qualitative assessment of the results using comparison of the data from Wu and Porté-Agel.[20] Qualitative comparison of wake-snapshots with the data of Churchfield et al.[7] also reveal the meandering nature of the wakes when seen from streamwise-spanwise plane. It is also important to note that the periodic streamwise boundary conditions in the AL model manifest essentially an array of turbine placed in the streamwise direction with a period of 4π.

The future work involves using atmospheric boundary layer simulations to be supplied as inflow conditions in actuator line models to generate more feasible results which is currently under way, and using realistic boundary conditions in large wind-farm simulations.

VI. Acknowledgements

The authors would like to acknowledge the support of NSF-CBET 13358568 grant for the present work.

References

[1]Pope, S. B., *Turbulent Flows*, Cambridge Press, 2000.

[2]Chapman, D., "Computational aerodynamics, development and outlook," *AIAA J.*, Vol. 17, 1979, pp. 1293–313.

[3]Reynolds, W. C., "The potential and limitations of direct and large eddy simulations," *Lecture Notes in Physics*, Vol. 357, J. L. Lumlery, Ed., Springer-Verlag, Berlin, 1990, pp. 313–343.

[4]Ivanell, S. S. A., *Numerical Computations of Wind Turbine Wakes*, Ph.D. thesis, Dept. of Mechanics, Gotland Univ., Stockholm, Sweden, 2010.

[5]Calaf, M., Meneveau, C., and Meyers, J., "Large Eddy Simulation Study of Fully Developed Wind-Turbine Array Boundary Layers," *Phys. Fluids*, Vol. 22, 2010, pp. 015110.

[6]Porté-Agel, F., Wu, Y.-T., and Conzemius, R. J., "Large-Eddy Simulation of Atmospheric Boundary Layer Flow Through Wind Turbines and Wind Farms," *J. of Wind Eng. and Ind. Aerodynamics*, Vol. 99, 2011, pp. 154–168.

[7]Churchfield, M. J., Lee, S., Moriarty, P. J., Martinez, L. A., Leonardi, S., Vijayakumar, G., and Brasseur, J. G., "A Large-Eddy Simulation of Wind-Plant Aerodynamics," AIAA Paper 2012-0537, 2012.

[8]Churchfield, M. J., Michalakes, J., and Moriarty, P. J., "A Numerical Study of the Effects of Atmospheric and Wake Turbulence on Wind Turbine Dynamics,," *J. Turb.*, Vol. 13, No. 14, 2012, pp. 1–32.

[9]Rankine, W. J. M., "On the Mechanical Principles of the Action of Propellers." *Trans. Inst. Naval Architects*, Vol. 6, 1865.

[10]Glauert, H., "Airplane Propellers," *Aerodynamic Theory*, ed. W. F. Durand, New York 4, Div. L, 1963, pp. 128–143.

[11]Jimenez, A., Crespo, A., Migoya, F., and Garcia, J., "Large-eddy simulation of spectral coherence in a wind turbine wake," *Env. Research Letters*, Vol. 3, 2008.

[12]Sørensen, J. N. and Myken, A., "Unsteady actuator disc model for horizontal axis wind turbines," *J. of Wind Eng. and Ind. Aerodynamics*, Vol. 39, 1992, pp. 139–149.

[13]Mikkelsen, R., *Actuator Disc Methods Applied to Wind Turbines*, Ph.D. thesis, Technical University of Denmark, 2003.

[14]Sorensen, J. N. and Shen, W. Z., "Numerical modelling of Wind Turbine Wakes," *J. Fluids Eng.*, Vol. 124, 2002, pp. 393–399.

[15]Troldborg, N., *Actuator Line Modeling of Wind Turbine Wakes*, Ph.D. thesis, Technical University of Denmark, 2008.

[16]Spalart, P. R., "Direct Simulation of turbulent boundary layer up to $Re_\theta = 1400$," *J. Fluid. Mech.*, Vol. 187, 1988, pp. 61–98.

[17]Lund, T. S., Wu, X., and Squires, K. D., "Generation of turbulent Inflow data for Spatially-Developing Boundary Layer Simulations," *J. Comp. Physics*, Vol. 140, 1998, pp. 233–258.

[18]Ferrante, A. and Elghobashi, S. E., "A robust method for generating inflow conditions for direct simulations of spatially developing turbulent boundary layers," *J. Comp. Physics*, Vol. 198, 2004, pp. 372–387.

[19]Stoll, R. and Porté-Agel, F., "Dynamic subgrid-scale models for momentum and scalar fluxes in large-eddy simulations of neutrally stratified atmospheric boundary layers over heterogeneous terrain," *Water Resources Research*, Vol. 42, 2006, pp. W01409.

[20]Wu, Y.-T. and Porté-Agel, F., "Large-Eddy Simulation of Wind-Turbine Wakes: Evaluation of Turbine Parametrisations," *Boundary Layer Metereol*, Vol. 138, 2011, pp. 345–366.

[21]Deardorff, J. W., "A numerical study of three-dimensional turbulent channel flow at large Reynolds number," *J. Fluid. Mech.*, Vol. 41, 1970, pp. 453–480.

[22]Schumann, U., "Subgrid scale model for finite difference simulations of turbulent flows in plane channels and annuli," *J. Comp. Phys.*, Vol. 18, 1975, pp. 376–404.

[23]Porté-Agel, F., Meneveau, C., and Parlange, M. B., "A scale-dependant dynamic model for large eddy simulation: application to a neutral atmospheric boundary layer," *J. Fluid. Mech.*, Vol. 17, 2000, pp. 261–284.

[24]Fischer, P., "An Overlapping Schwarz Method for Spectral Element Solution of the Incompressible NavierStokes Equations," *J. Comp. Phys.*, Vol. 133, 1997, pp. 84–101.

[25]Orszag, S. A., "Transform method for calculations of vector coupled sums: Application to the spectral form of vorticity equation," *J. Atmos. Sci.*, Vol. 27, 1970, pp. 890–895.

[26]Canuto, C. M., Hussaini, Y., Qaurteroni, A., and Zhang, T. A., *Spectral Methods in Fluid Dyanamics*, New York: Springer, 8th ed., 1988.

[27]Fischer, P., Lottes, J., Pointer, D., and Siegel, A., "Petascale Algorithms for Reactor Hydrodynamics,," *J. Phys. Conf. Series*, 2008.

[28] "Mathematics and Computer Science Division, Argonne National Laboratory," http://www.mcs.anl.gov/.

[29]Meyers, J. and Sagaut, P., "On the Model Coefficient for the Standard and the Variational Multi-Scale Smagorinsky Model," *J. Fluid Mech.*, Vol. 569, 2006, pp. 287–319.

[30]Moeng, C., "A large-eddy-simulation model for the study of planetary boundary-layer turbulence," *J Atmos Sci.*, Vol. 41, 1984, pp. 2052–2062.

[31]Businger, J. A., Wyngaard, J. C., Izulmi, Y., and Bradley, E., "Flux profile relationships in the atmospheric surface layer," *J Atmos Sci.*, Vol. 28, 1971, pp. 181–189.

[32]Monin, A. S. and Obukhov, A. M., "Basic Laws of Turbulent Mixing in the Ground Layer of the Atmosphere," *Trans. Geophys. Inst. Akad. Nauk. USSR*, Vol. 151, 1954, pp. 163–187.

[33]Schlichting, H., *Boundary-layer theory*, Berlin; New York: Springer, 8th ed., 2000.

[34]Bou-Zeid, E., Meneveau, C., and Parlange, M., "A scale-dependant Lagrangian dynamic model for large eddy simulation of complex turbulent flows," *Phys. Fluids*, Vol. 415, 2005, pp. 025125.

[35]Mason, P. J. and Thompson, D. J., "Stochastic backscatter in large-eddy simulations of boundary layers," *J. Fluid. Mech.*, Vol. 242, 1992, pp. 51–78.

[36]Castro, I. P., Segalini, A., and Alfredsson, P. H., "Outer Layer Turbulence Intensities in smooth and rough-wall boundary layers," *J. Fluid. Mech.*, Vol. 727, 2013, pp. 119–131.

[37]Bhaganagar, K., Kim, J., and Coleman, G., "Effect of Roughness on Wall-Bounded Turbulence," *Flow,Turbulence and Combustion*, Vol. 72, 2004, pp. 463–492.

[38]Jiménez, J., "Turbulent Flows over Rough Walls," *Annu. Rev. Fluid. Mech.*, Vol. 36, 2004, pp. 173–196.

[39]Patil, S. and Tafti, D., "Two Layer Wall Model for Large-Eddy Simulations of Flow over Rough Surfaces," *AIAA journal*, Vol. 50, 2012, pp. 454–460.

[40]Meneaveau, C. and Katz, J., "Scale-invariance and turbulence models for large eddy simulation of boundary layers," *Ann. Rev. Fluid. Mech.*, Vol. 32, 2000, pp. 1–32.

[41]Fischer, P. F., Lottes, J. W., and Kerkemeier, S. G., "nek5000 Web page," 2008, http://nek5000.mcs.anl.gov.

[42]Peet, Y., Fischer, P., Conzelmann, G., and Kotamarthi, V., "Actuator Line Aerodynamics model with Spectral Elements," AIAA paper 2013–1210, 2013, 07 - 10 January 2013, Grapevine (Dallas/Ft. Worth Region), Texas.

[43]Martinez, L. A., Leonardi, S., Churchfield, M. J., and Moriarty, P. J., "A Comparison of Actuator Disk and Actuator Line Wind Turbine Models and Best Practices for Their Use," AIAA Paper 2012-0900, 2012.

[44]Chamorro, L. P. and Porté-Agel, F., "A Wind-Tunnel Investigation of Wind-Turbine Wakes: Boundary-Layer Turbulence Effects," *Boundary Layer Metereol*, Vol. 132, 2009, pp. 129–149.

[45]Fischer, P. and Mullen, J., "Filter-based stabilization of spectral element methods," *Comptes rendus de lAcadémie des sciences, Série I- Analyse numérique*, Vol. 332, 2001, pp. 265–270.